Research Article | Vol. 30, No. 19 / 12 Sep 2022 / Optics Express 34378
Optics EXPRESS

Optical multi-trapping by Kinoform m-Bonacci lenses

FRANCISCO M. MUÑOZ-PÉREZ,[1,2,*] VICENTE FERRANDO,[1] WALTER D. FURLAN,[3] JUAN A. MONSORIU,[1] AND J. RICARDO ARIAS-GONZALEZ[1]

[1] *Centro de Tecnologías Físicas, Universitat Politècnica de València, E- 46022, València, Spain*
[2] *Laboratorio de Fibra Óptica, Universidad Politècnica de Tulancingo, División de Posgrado, Hidalgo, Mexico*
[3] *Departamento de Óptica, Universitat de València, Burjassot, E- 46100, Spain*
[*] *fmmuope1@upvnet.upv.es*

Abstract: Optical manipulation is interfacing disciplines in the micro and nanoscale, from molecular biology to quantum computation. Versatile solutions for increasingly more sophisticated technological applications require multiple traps with which to maneuver dynamically several particles in three dimensions. The axial direction is usually overlooked due to difficulties in observing particles away from an objective-lens focal plane, a normal element in optical tweezers, and in managing interparticle distances along the trapping beam propagating direction, where strong radiation pressure and shadowing effects compromise the simultaneous and stable confinement of the particles. Here, aperiodic kinoform diffractive lens based on the m-Bonacci sequence are proposed as a new trapping strategy. This lens provides split first-order diffractive foci whose separation depends on the generalized m-golden ratio. We show the extended manipulation capabilities of a laser tweezers system generated by these lens, in which concomitant trapping of particles in different focal planes takes place. Positioning particles in the axial direction with computer-controlled distances allows dynamic three-dimensional all-optical lattices, useful in a variety of microscale and nanoscale applications.

1. Introduction

With the advent of nanoscience, laser manipulation is becoming a key tool in multiple areas of interdisciplinary science, such as molecular biophysics, condensed matter and quantum technologies [1–4]. A wealth of trapping designs to control micro and nanostructures are being generated with specific features that enable atom cooling, particle confinement, thermodynamic descriptions of molecular motors away from equilibrium or single-molecule mechano-chemical analyses of nucleic acids, proteins and viruses, to name a few [5–10]. Optical tweezers are a versatile instrument with which to confine structures, measure forces (down to femto Newtons) and distances (in the subnanometer range), detect temperature gradients or scan structures in physiological environments to a high resolution [11–15]. In the last decade, structured beams have expanded the maneuvering capabilities of this instrument: elliptically polarized beams and the generation of vortices enable particle rotation [16–18], and both interferometric and holographic methods demonstrate simultaneous control on multiple particles [19,20]. In this regard, the use of spatial light modulators with which to model the phase of the beam largely increases the flexibility in beam-structure designs for optical tweezers [21].

On the other hand, a renewed interest in diffractive optical elements has been raised in the last decades due to their capability to boost novel devices in the optical range [22,23] and other electromagnetic windows [24–26]. Diffractive lenses based on fractal aperiodic sequences present interesting properties for the generation of multiple foci with an extended depth of field [27–29]. The design of new multifocal diffractive lenses using other aperiodic sequences, such as the

#465672 https://doi.org/10.1364/OE.465672
Journal © 2022 Received 1 Jun 2022; revised 2 Aug 2022; accepted 11 Aug 2022; published 6 Sep 2022

Optics EXPRESS

Thue-Morse [30] sequence or Walsh functions [23], is also possible. We previously introduced a new diffractive bifocal structure, the Fibonacci Zone Plates (FZP) based on the Fibonacci sequence, and proved both theoretically and experimentally that an FZP provides a pair of foci whose separation depends on the golden ratio under monochromatic plane wave illumination [31]. We then proposed a generalization of the FZP, the so-called m-Bonacci [32]. Since it is possible to generate multiple optical vortices by combining aperiodic lenses with a helical phase mask [33], the incorporation of these diffractive elements offer great flexibility in the design and applications of optical tweezers systems [34,35].That is why the implementation of diffractive lenses is a highly efficient option in the development of new optical tweezers setup.

In this work, we design and implement an optical tweezers system with a Kinoform m-Bonacci lens. After introducing the theoretical basis and focusing properties of the lenses, we show that the diffractive properties of these lenses allow multiple trapping and simultaneous three-dimensional manipulation of particles at different focal planes with controlled separation. We end up by discussing applications in which our trapping strategy could lead to technological solutions in interdisciplinary fields.

2. Kinoform m-Bonacci lens design

The Kinoform m-Bonacci Lenses (KmBLs) are diffractive pure phase elements based on the m-Bonacci sequence, a generalization of the Fibonacci sequence [32]. The m-Bonacci set of numbers are obtained from m given elements $N_{m,0} = 0$, $N_{m,1} = 1$, and $N_{m,j} = \sum_{i=1}^{j} N_{m,j-1}$ with $1<j<m$. From these seed elements, the S^{th} element of the m-Bonacci set of numbers is obtained by applying the iteration rule $N_{m,S} = \sum_{i=1}^{m} N_{m,S-1}$ with $S \geq m$. As an example, to define the Tribonacci numbers serie, we start from the first m elements as seeds: $N_{3,0} = 0$, $N_{3,1} = 1$, and $N_{3,2} = N_{3,0} + N_{3,1} = 1$. Then, the next Tribonacci numbers ($S>3$) are obtained by applying the iteration rule $N_{3,i} = N_{3,i-1} + N_{3,i-2} + N_{3,i-3}$, so $N_{3,i} = \{0, 1, 1, 2, 4, 7, 13, 24, 44 \cdots\}$. Given the m-Bonacci series, the generalized golden number or golden ratio is defined as the limit in the proportion between two consecutive m-Bonacci numbers:

$$\varphi_m = \lim_{S\to\infty} \frac{N_{m,S}}{N_{m,S-1}} \tag{1}$$

resulting $\varphi_2 = 1.618$ for the Fibonacci series ($m = 2$), i.e, the well-known golden ratio, whereas for Tribonacci ($m = 3$) and Tetranacci ($m = 4$) series the corresponding generalized m-golden ratio are $\varphi_3 = 1.839$ and $\varphi_4 = 1.927$, respectively.

Following a similar procedure, it is possible to generate a binary m-Bonacci sequence starting from m given seed elements and the concatenation of the previous ones $t_{m,j} = \{t_{m,j-1}\, t_{m,j-2} \cdots t_{m,0}\}$ with $1<j<m$. Then, higher order $S \geq m$ sequences are obtained by concatenating the preceding m elements, $t_{m,S} = \{t_{m,S-1}\, t_{m,S-2} \cdots t_{m,S-m}\}$. To obtain the $m = 3$ sequence, in accord with the Tribonacci example, we start from the seed elements $t_{3,0} = \{B\}$, $t_{3,1} = \{A\}$ and $t_{3,2} = \{AB\}$. Then, the successive order sequences are constructed by applying the concatenation rule $t_{3,S} = \{t_{3,S-1}, t_{3,S-2}, t_{3,S-3}\}$, obtaining $t_{3,3} = \{ABAB\}$, $t_{3,4} = \{ABABABA\}$, $t_{3,5} = \{ABABABAABABAB\}$, and so on.

In order to design a KmBL, we have to note that two successive elements "B" are separated by either one or two "A" elements in any given sequence $t_{m,S}$. These sequences can be used to define the generating function, $\Phi(\zeta)$, for the quadratic radial phase distribution of the lens: $\Phi(\zeta)$ is a function with compact support in the interval $[0, 1]$ that varies linearly between $\Phi = 0$ rad and $\Phi = 2\pi$ rad at each sub-interval $\{AB\}$ of the sequence and becomes $\Phi(\zeta) = 0$ rad otherwise (see Fig. 1(a)).

The radial surface-relief profile of the KmBL with $m = 3$ and $S = 6$ is shown in Fig. 1(b). The normalized squared radial coordinate is defined as $\zeta = (r/a)^2$, where r is the radial coordinate of

Optics EXPRESS

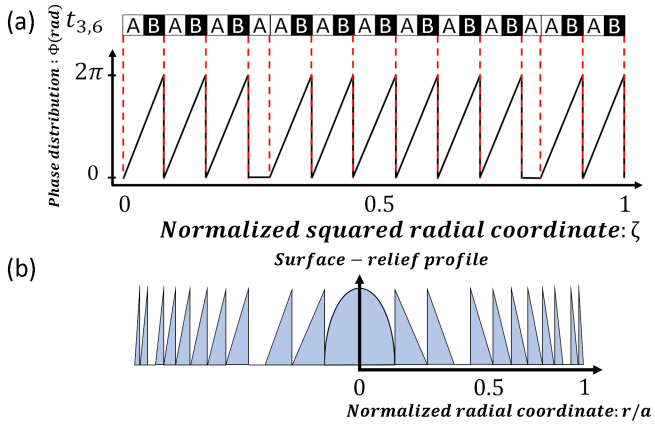

Fig. 1. (a) Construction of the KmBL phase profile from the $t_{3,6}$ sequence represented in the normalized square radial coordinate. (b) Surface-relief profile of the KmBL with $m = 3$ and order $S = 6$.

the lens and a is the external radius. The KmBL profile can present as a Fresnel kinoform lens with an aperiodic distribution of half-period defects.

3. Focusing properties

To evaluate the focusing properties of KmBLs, we have computed the axial irradiance under monochromatic plane wave illumination by using the Fresnel approximation:

$$I(u) = 4\pi u^2 \left| \int_0^1 t(\zeta) \exp(-2\pi i u \zeta) d\zeta \right|^2 \tag{2}$$

where $u = a^2/2\lambda z$ is the reduced axial coordinate, λ is the wavelength of the light, z is the focal length, and $t(\zeta) = \exp|i\Phi(\zeta)|$ is the transmittance function, being $\Phi(\zeta)$ the phase of the lens.

Figure 2 shows the KmBL axial irradiances for Fibonacci ($m = 2$, $S = 12$, $a = 6.99$ mm), Tribonacci ($m = 3$, $S = 10$, $a = 7.11$ mm) and Tetranacci ($m = 4$, $S = 9$, $a = 6.05$ mm) series. The KmBLs provide a pair of foci whose vergences can be related to the generalized m-golden ratio. For the three lenses herein studied, the order S and the lens radius a have been tuned to provide the intermediate position between foci at the same axial position. Focal planes are located at $f_a = 3.87$ D and $f_b = 2.39$ D for Fibonacci, $f_a = 3.4$ D and $f_b = 2.87$ D for Tribonacci and $f_a = 3.26$ D and $f_b = 3.007$ D for Tetranacci.

The locations of the focal points change as the order m increases, making the distance between the focal planes shrink. This is an important, common feature of the three lenses, along with the fact that the focal length ratio, f_a/f_b, approaches $1/(\varphi_m - 1)$, with φ_m the generalized golden number mentioned above.

Optics EXPRESS

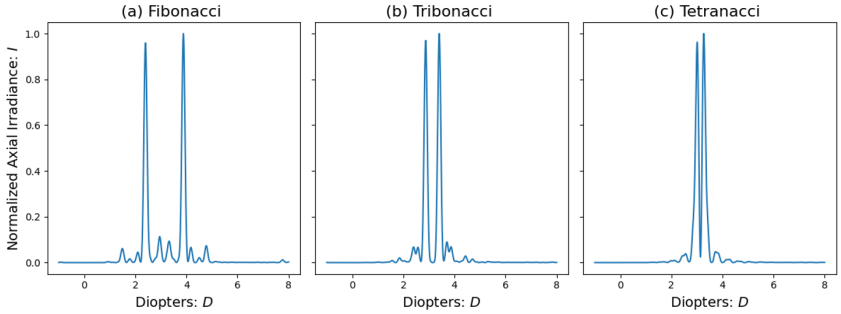

Fig. 2. Normalized axial irradiance generated by three KmBL lenses. (a) Fibonacci ($m = 2, S = 12$), (b) Tribonacci ($m = 3$, $S = 10$) and (c) Tetranacci ($m = 4$, $S = 9$).

4. Experimental results

We implemented an optical tweezers setup to show the trapping capabilities of the above design, with diagram depicted in Fig. 3. A beam is emitted from a CW laser ($\lambda = 1064$ nm, Laser Quantum, Mod. Opus 1064) with a maximum power of 3 W. A half-wave plate ($\lambda/2$) is placed at the laser output followed by a linear polarizer (P), which changes the direction of the beam linear polarization. The laser beam is then redirected by mirrors ($M1$ and $M2$) and expanded through a system of magnification 3, formed by lenses $L1$ and $L2$ (focal length $f_1 = 50$ mm and $f_2 = 150$ mm). The KmBL was projected on a spatial light modulator (SLM) (Holoeye PLUTO-2.1-NIR-149, phase-type, pixel size 8 μm and resolution 1920 x 1080 pixels) screen. The SLM is configured for a 2.1π phase at a wavelength $\lambda = 1064$ nm. The resulting KmBL beam, as modulated at the SLM, is reduced by a $4f$ system formed by $L3$ ($f_3 = 150$ mm) and $L4$ (focal length $f_4 = 150$ mm).

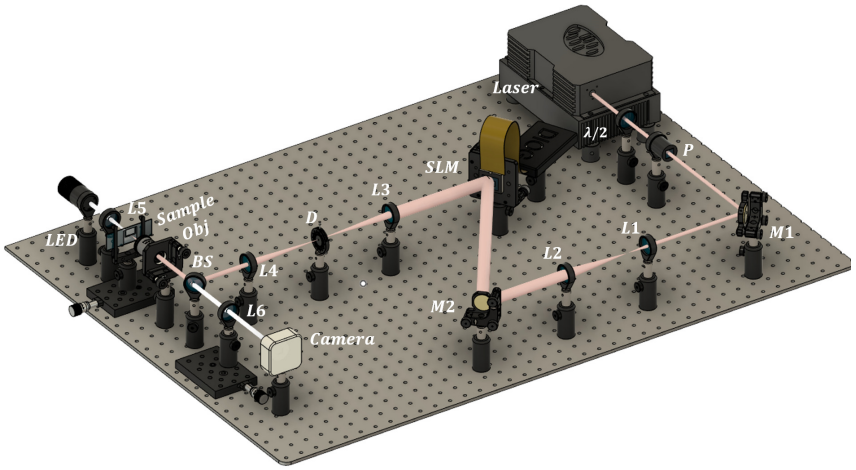

Fig. 3. Experimental setup for trapping and manipulation of particles using kinoform m-bonacci lens-based laser tweezers.

A 1D blazed grating is added to each KmBL, which purpose is to act as a linear phase carrier. It allows the diffracted light to be conducted towards the first order of diffraction, thus preventing noise caused by specular reflection from higher diffraction orders. More in depth, the beam is spatially filtered by a diaphragm (D) placed at the focal point of $L3$, thus allowing only the first order to pass. The added linear phase carrier is offset by slightly tilting the SLM, making the first

Optics EXPRESS

order of diffraction align with the diaphragm's optical axis. Then, the KmBL image is passed through a high-numerical aperture oil-immersion objective (Olympus UPLFLN 100X, NA= 1.3), placed at the $L4$ focal plane. An LED light source (Thorlabs, Mounted High-Power, 1300 mA, Mod. MCWHL7) is included to illuminate the sample; its light is collimated and then focused on the sample through lens $L5$ (f_5 = 30 mm). Finally, a Beam Splitter (BS) is used to transmit visible light from the sample through the objective's back focal plane. The BS prevents reflections of infrared light from being transmitted to the imaging system. The resulting image is focused with lens L_6 (f_6 = 50 mm). A CMOS camera sensor (Edmund Optics, Mod. EO-10012C) is used to capture the images.

We next analyze the experimental results that demonstrate trapping and manipulation of microparticles in the focal planes of the KmBLs. Figure 4 displays the stable trapping of two polystyrene microparticles (diameter ~ 2 μm) using three different orders of KmBL (Fibonacci m = 2, Tribonacci m = 3, and Tetranacci m = 4). The first particle is indicated by a red arrow and the second by a green arrow. As theoretically predicted, the formation of two focal planes by KmBL allows multiple trapping of microparticles but the three KmBLs have the same focusing distance and the middle position of the split foci remains at the same spatial position for the three cases shown in Fig. 4. The functional relation between both foci makes it possible to control the distance that separates the particles; namely, by increasing the number m, the distance between the foci decreases. In this regard, the trapping positions are Z_a = 6.779 mm and Z_b = 6.847 mm for Fibonacci, Z_a = 6.801 mm and Z_b = 6.825 mm for Tribonacci and Z_a = 6.807 mm and Z_b = 6.819 mm for Tetranacci, which provide separations between the particles of 68.7 μm for Fibonacci, 24.60 μm for Tribonacci, and 11.7 μm for Tetranacci. As shown in Fig. 4(ac), the microparticles are trapped with the greatest separation for m = 2, a distance that decreases for m = 3 and m = 4. It is important to mention that the high numerical aperture lens performs a rescaling of the focal points, that is, the power of the objective (P_O = 555 D or ~ 150 D in distilled water) modifies the axial distances of the foci. The oblique incidence of the beam provides a shift of the axial points in the transversal plane, so it facilitates the observation of both particles in different planes.

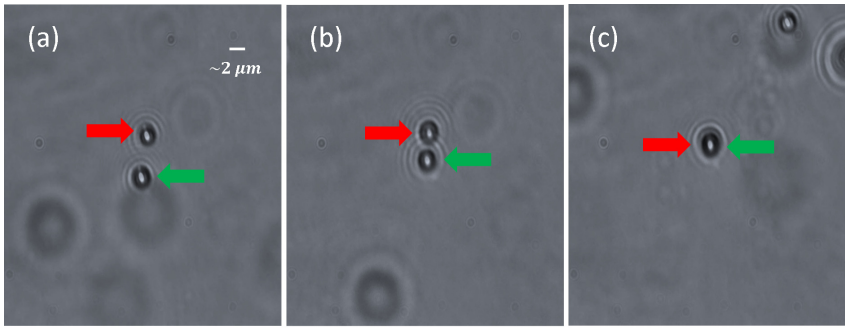

Fig. 4. Particle trapping through Kinoform m-Bonacci Lens (KmBL) based on optical tweezers. (a) Fibonacci (m = 2, S = 12) (see Visualization 1), (b) Tribonacci (m = 3, S = 10) (see Visualization 2), and (c) Tetranacci (m = 4, S = 9) (see Visualization 3).

The distance between the particles is considerably smaller for Tribonacci KmBL, Fig. 4(b), relative to Fibonacci KmBL, Fig. 4(a). The Tetranacci KmBL case presents the smallest distance between the particles for the three KmBLs, see Fig. 4(c); in fact, the focal planes are so close that the particle in the foreground almost hides the view of the other particle behind.To ascertain these descriptions, Visualization 1, Visualization 2, and Visualization 3 show the trapping and multiple manipulations of the particles in greater detail.

Optics EXPRESS

5. Conclusions

We have designed and implemented a kinoform m-Bonacci lens-based optical tweezers system, with which to trap multiple particles along the optical axis. These lenses generate two main foci, which focal distance ratio is related to the order parameter. The trapping ability of the Fibonacci ($m = 2$), Tribonacci ($m = 3$), and Tetranacci ($m = 4$) lenses exhibit stable confinement of two particles and the possibility to control the distance between them. In contrast to the diffractive design used in Ref. [35], which generates a binary fractal profile with a set of traps in different axial positions and intensities, the m-Bonacci kinoform lens produces a pair of foci with equivalent intensities whose positions are determined by the m-golden ratio. This confers similar stability to the trapped particles and affords the control of the distance between the optical traps through the order m.

Kinoform m-Bonacci lenses open an alternative way to full, three-dimensional manipulation by optical arrangements with dynamic control on the trapping positions. In this regard, apart from continuous motion, stepping motion in the axial direction —where particles switch between discrete, transversal planes over which manipulation is continuously driven— could be induced. This is a desired competence in single-molecule experiments because it allows testing sudden configurational changes in biochemical reactions, within a background of thermal fluctuations. In addition, the fact that the axial direction is strictly more defined than the transversal ones in an optical setup affords higher precision in positioning nanoparticles along a line at controlled distances, useful to explore their mutual interactions under laser irradiation. Finally, we believe that the extension of our axially-generated multiplexed trapping to several beams —enabling three-dimensional optical lattices— will find applications as architectures for quantum computation.

Funding. Ministerio de Ciencia e Innovación (PID2019-107391RB-I00); Generalitat Valenciana (PROMETEO/2019/048); Universitat Politècnica de València (PAID-01-20-25).

Acknowledgments. This work was supported by the Ministerio de Ciencia e Innovación de España (grant PID2019-107391RB-I00) and by Generalitat Valenciana (grant PROMETEO/2019/048), Spain. F.M.M.P also acknowledgment the financial support from the Universitat Politècnica de València (PAID-01-20-25), Spain.

Disclosures. The authors declare no conflicts of interest.

Data availability. Data underlying the results presented in this paper are not publicly available at this time but may be obtained from the authors upon reasonable request.

References

1. H. Xin, Y. Li, Y.-C. Liu, Y. Zhang, Y.-F. Xiao, and B. Li, "Optical forces: From fundamental to biological applications," Adv. Mater. **32**(37), 2001994 (2020).
2. S. Hu, Z. Liao, L. Cai, and X. Jiang, "Near-field optical tweezers for chemistry and biology," Phys. Status Solidi A **217**(1), 1900604 (2020).
3. C. J. Bustamante, Y. R. Chemla, S. Liu, and M. D. Wang, "Optical tweezers in single-molecule biophysics," Nat. Rev. Methods Primers **1**(1), 25 (2021).
4. C. Weitenberg, S. Kuhr, K. Mölmer, and J. F. Sherson, "Quantum computation architecture using optical tweezers," Phys. Rev. A **84**(3), 032322 (2011).
5. A. Kaufman and K. Ni, "Quantum science with optical tweezer arrays of ultracold atoms and molecules," Nat. Phys. **17**(12), 1324–1333 (2021).
6. Y. Shi, K. T. Nguyen, L. K. Chin, Z. Li, L. Xiao, H. Cai, W. H. R. Yu, S. Feng, P. H. Yap, J. Liu, Y. Zhang, and A. Q. Liu, "Trapping and detection of single viruses in an optofluidic chip," Acs. Sens. **6**(9), 3445–3450 (2021).
7. M. L. Juan, M. Righini, and R. Quidant, "Plasmon nano-optical tweezers," Nat. Photonics **5**(6), 349–356 (2011).
8. I. A. Martínez, E. Roldán, L. Dinis, and R. A. Rica, "Colloidal heat engines: a review," Soft Matter **13**(1), 22–36 (2017).
9. J. R. Arias-Gonzalez, "Single-molecule portrait of dna and rna double helices," Integr. Biol. **6**(10), 904–925 (2014).
10. J. R. Arias-Gonzalez, "Optical tweezers to study viruses," Subcell. Biochem. **68**, 273–304 (2013).
11. I. Stoev, B. Seelbinder, and E. Erben, "Highly sensitive force measurements in an optically generated, harmonic hydrodynamic trap," eLight **1**(1), 7 (2021).
12. H. Rodríguez-Rodríguez, G. Salas, and J. R. Arias-Gonzalez, "Heat generation in single magnetic nanoparticles under near-infrared irradiation," J. Phys. Chem. Lett. **11**(6), 2182–2187 (2020).

Optics EXPRESS

13. H. Rodríguez-Rodríguez, M. Acebron, F. J. Iborra, J. R. Arias-Gonzalez, and B. H. Juarez, "Photoluminescence activation of organic dyes via optically trapped quantum dots," ACS Nano **13**(6), 7223–7230 (2019).
14. S. de Lorenzo, M. Ribezzi-Crivellari, J. R. Arias-Gonzalez, S. B. Smith, and F. Ritort, "A temperature-jump optical trap for single molecule manipulation," Biophys. J. **108**(12), 2854–2864 (2015).
15. A. A. A. Balushi, A. Kotnala, S. Wheaton, R. M. Gelfand, Y. Rajashekara, and R. Gordon, "Label-free free-solution nanoaperture optical tweezers for single molecule protein studies," Analyst **140**(14), 4760–4778 (2015).
16. M. Padgett and R. Bowman, "Controlled rotation of optically trapped microscopic particles," Science **292**(5518), 912–914 (2001).
17. M. Padgett and R. Bowman, "Tweezers with a twist," Nat. Photonics **5**(6), 343–348 (2011).
18. J. R. Arias-Gonzalez and M. Nieto-Vesperinas, "Radiation pressure over dielectric and metallic nanocylinders on surfaces: polarization dependence and plasmon resonance conditions," Opt. Lett. **27**(24), 2149–2151 (2002).
19. P. Jákl, T. Cižmár, M. Šerý, and P. Zemáne, "Static optical sorting in a laser interference field," Appl. Phys. Lett. **92**(16), 161110 (2008).
20. P. Chiou, A. Ohta, and M. Wu, "Massively parallel manipulation of single cells and microparticles using optical images," Nature **436**(7049), 370–372 (2005).
21. J. Gieseler, J. Gomez-Solano, A. Magazzú, I. P. Castillo, L. P. García, M. Gironella-Torrent, X. Viader-Godoy, F. Ritort, G. Pesce, A. Arzola, K. Volke-Sepulveda, and G. Volpe, "Optical tweezers: A comprehensive tutorial from calibration to applications," Adv. Opt. Photonics **13**(1), 74–241 (2021).
22. W. D. Furlan, D. Montagud, V. Ferrando, S. Garcia-Delpech, and J. A. Monsoriu, "A new trifocal corneal inlay for presbyopia," Sci. Rep. **11**(1), 6620 (2021).
23. F. Machado, V. Ferrando, F. Giménez, W. D. Furlan, and J. A. Monsoriu, "Multiple-plane image formation by walsh zone plates," Opt. Express **26**(16), 21210–21218 (2018).
24. I. Mohacsi, I. Vartiainen, B. Rösner, M. Guizar-Sicairos, V. A. Guzenko, I. McNulty, R. Winarski, M. V. Holt, and C. David, "Interlaced zone plate optics for hard x-ray imaging in the 10 nm range," Sci. Rep. **7**(1), 43624 (2017).
25. W. D. Furlan, V. Ferrando, J. A. Monsoriu, P. Zagrajek, E. Czerwińska, and M. Szustakowski, "3d printed diffractive terahertz lenses," Opt. Lett. **41**(8), 1748–1751 (2016).
26. L. Remon, S. Garcia-Delpech, P. Udaondo, V. Ferrando, J. A. Monsoriu, and W. D. Furlan, "Fractal-structured multifocal intraocular lens," PLoS One **13**(7), e0200197 (2018).
27. G. Saavedra, W. D. Furlan, and J. A. Monsoriu, "Fractal zone plates," Opt. Lett. **28**(12), 971–973 (2003).
28. W. D. Furlan, G. Saavedra, and J. A. Monsoriu, "White-light imaging with fractal zone plates," Opt. Lett. **32**(15), 2109 (2007).
29. F. Giménez, W. D. Furlan, A. Calatayud, and J. A. Monsoriu, "Multifractal zone plates," J. Opt. Soc. Am. A **27**(8), 1851–1855 (2010).
30. V. Ferrando, F. Giménez, W. D. Furlan, and J. A. Monsoriu, "Bifractal focusing and imaging properties of thue-morse zone plates," Opt. Express **23**(15), 19846 (2015).
31. J. A. Monsoriu, A. Calatayud, L. Remon, W. D. Furlan, G. Saavedra, and P. Andrés, "Bifocal fibonacci diffractive lenses," IEEE Photonics J. **5**(3), 3400106 (2013).
32. F. Machado, V. Ferrando, W. D. Furlan, and J. A. Monsoriu, "Diffractive m-bonacci lenses," Opt. Express **25**(7), 8267–8273 (2017).
33. A. Calatayud, V. Ferrando, F. Gimenez, W. D. Furlan, G. Saavedra, and J. A. Monsoriu, "Fractal square zone plates," Opt. Commun. **286**, 42–45 (2013).
34. J. Pu and P. H. Jones, "Devil's lens optical tweezers," Opt. Express **23**(7), 8190–8199 (2015).
35. X. Z. S. Cheng, W. Ma, and S. Tao, "Fractal zone plate beam based optical tweezers," Sci. Rep. **6**(1), 34492 (2016).